The Astronomical Journal, 155:78 (6pp), 2018 February https://doi.org/10.3847/1538-3881/aaa293
© 2018. The American Astronomical Society. All rights reserved.

Combining *Spitzer* Parallax and Keck II Adaptive Optics Imaging to Measure the Mass of a Solar-like Star Orbited by a Cold Gaseous Planet Discovered by Microlensing

J.-P. Beaulieu[1,2], V. Batista[2], D. P. Bennett[3], J.-B. Marquette[2,4], J. W. Blackman[1], A. A. Cole[1], C. Coutures[2], C. Danielski[5], D. Dominis Prester[6], J. Donatowicz[7], A. Fukui[8], N. Koshimoto[9], K. Lončarić[6], J. C. Morales[10], T. Sumi[7], D. Suzuki[3], C. Henderson[11,12,13], Y. Shvartzvald[11,14], and C. Beichman[12]
[1] School of Natural Sciences, University of Tasmania, Private Bag 37 Hobart, Tasmania 7001 Australia
Jeanphilippe.beaulieu@utas.edu.au, Andrew.Cole@utas.edu.au
[2] Sorbonne Universités, UPMC Université Paris 6 et CNRS, UMR 7095, Institut dAstrophysique de Paris, 98 bis bd Arago, F-75014 Paris, France; beaulieu@iap.fr
[3] Laboratory for Exoplanets and Stellar Astrophysics, NASA/Goddard Space Flight Center, Greenbelt, MD 20771, USA
[4] Laboratoire d'Astrophysique de Bordeaux, Univ. Bordeaux, CNRS, B18N, allée Geoffroy Saint-Hilaire, F-33615 Pessac, France
[5] GEPI Observatoire de Paris, Section de Meudon 5, place Jules Janssen F-92195 Meudon, France
[6] Department of Physics, University of Rijeka, Radmile Matejčić 2, 51000 Rijeka, Croatia
[7] Technische Universitt Wien, Karlsplatz 13, A-1040 Wien, Austria
[8] Okayama Astrophysical Observatory, National Astronomical Observatory of Japan, Asakuchi, Okayama 719-0232, Japan
[9] Department of Earth and Space Science, Graduate School of Science, Osaka University, 1-1 Machikaneyama, Toyonaka, Osaka 560-0043, Japan
[10] Institut de Cincies de lEspai (CSIC-IEEC), Campus UAB, Carrer de Can Magrans s/n, E-08193 Cerdanyola del Valls, Spain; morales@ieec.uab.es
[11] Jet Propulsion Laboratory, California Institute of Technology, 4800 Oak Grove Drive, Pasadena, CA 91109, USA
[12] NASA Exoplanet Science Institute, California Institute of Technology, Jet Propulsion Laboratory, Pasadena, CA 91125, USA
[13] PAC/NExScI, Mail Code 100-22, Caltech, 1200 East California Boulevard, Pasadena, CA 91125, USA
Received 2017 September 3; revised 2017 November 20; accepted 2017 December 4; published 2018 January 23

Abstract

To obtain accurate mass measurements for cold planets discovered by microlensing, it is usually necessary to combine light curve modeling with at least two lens mass–distance relations. The physical parameters of the planetary system OGLE-2014-BLG-0124L have been constrained thanks to accurate parallax effect between ground-based and simultaneous space-based *Spitzer* observations. Here, we resolved the source+lens star from sub-arcsecond blends in H-band using adaptive optics (AO) observations with NIRC2 mounted on Keck II telescope. We identify additional flux, coincident with the source to within 160 mas. We estimate the potential contributions to this blended light (chance-aligned star, additional companion to the lens or to the source) and find that 85% of the NIR flux is due to the lens star at $H_{\rm L} = 16.63 \pm 0.06$ and $K_{\rm L} = 16.44 \pm 0.06$. We combined the parallax constraint and the AO constraint to derive the physical parameters of the system. The lensing system is composed of a mid-late type G main sequence star of $M_{\rm L} = 0.9 \pm 0.05\ M_{\odot}$ located at $D_{\rm L} = 3.5 \pm 0.2$ kpc in the Galactic disk. Taking the mass ratio and projected separation from the original study leads to a planet of $M_{\rm p} = 0.65 \pm 0.044\ M_{\rm Jupiter}$ at 3.48 ± 0.22 au. Excellent parallax measurements from simultaneous ground-space observations have been obtained on the microlensing event OGLE-2014-BLG-0124, but it is only when they are combined with ∼30 minutes of Keck II AO observations that the physical parameters of the host star are well measured.

Key words: gravitational lensing: micro – planetary systems – planets and satellites: detection

1. Mass–Distance Relations for Microlensing

Gravitational microlensing is unique in its sensitivity to exoplanets down to Earth mass beyond the snow line (Mao & Paczynski 1991; Gould & Loeb 1992), where the core accretion theory predicts that the most massive planets will form. However, the major limitation of most of the 51 exoplanetary microlensing analyses published to date has been the relatively low precision measurements of physical parameters of the system, owing to uncertainty of the host star mass and its distance. By contrast, the relative physical parameters (mass ratio, projected separation relative to the angular Einstein ring radius) are usually known with high precision. In the vast majority of microlensing events, the Einstein ring radius crossing time $t_{\rm E}$ is the only measurable parameter constraining the lens mass, lens distance, and relative lens-source proper motion $\mu_{\rm rel}$, which are therefore degenerate. For binary microlensing events, it is possible to accurately measure the mass ratio q and the projected separation d in units of Einstein ring radius. The source star often transits the caustic, providing the source radius crossing time t_*. Moreover, the angular radius of the source star θ_* can be estimated from the surface brightness relation (Kervella et al. 2004; Boyajian et al. 2013, 2014), so the measurement of t_* yields the angular Einstein radius, $\Theta_{\rm E} = \theta_*\, t_{\rm E}/t_*$.

These constraints lead to a mass–distance relation between lens mass M_L at distance D_L, with the form

$$M_{\rm L} = \theta_{\rm E}^2/(\kappa\, \pi_{\pm{\rm rel}}) \quad (1)$$

where $\pi_{\pm{\rm rel}} = ({\rm au})\,(D_{\rm S} - D_{\rm L})/(D_{\rm S}\, D_{\rm L})$ and $\kappa = 8.144\ {\rm mas}\ M_{\odot}^{-1}$.

There is also a relation between the parallax π_E and the mass,

$$M_{\rm L} = \theta_{\rm E}/(\kappa\, \pi_{\rm E}). \quad (2)$$

This allows the elimination of $\theta_{\rm E}$ to give a useful mass–distance relation for the case when we have well-defined

[14] NASA Postdoctoral Program Fellow.

parallax π_E but unknown θ_E:

$$M_L = \pi_{\pm rel}/(\kappa\, \pi_E^2) \quad (3)$$

An independent mass–distance relation can be applied if the flux from the lens system can be reliably measured and compared to stellar models. Using high angular resolution observations with Keck II, SUBARU, or *HST*, it is possible to separate the contributions of the source and lens stars from blended stars at the sub-arcsecond level. We can then measure the lens apparent magnitude $m_L(\lambda)$ and combine it with isochrones (e.g., Bertelli et al. 2008) to get another mass–distance relation:

$$m_L(\lambda) = 10 + 5\log(D_L/1\ \mathrm{kpc}) + A_L(\lambda) + M_{\mathrm{isochrone}}(\lambda, M_L, \mathrm{age}, [\mathrm{Fe/H}]) \quad (4)$$

where $M_{\mathrm{isochrone}}$ is the predicted absolute magnitude of the lens assuming a given mass, age, and metallicity, and $A_L(\lambda)$ is the wavelength-dependent interstellar extinction along the line of sight to the lens.

In practice, the parallax vector is often not well constrained and there is a degeneracy with orbital motion, while the Einstein ring radius is usually known to about 10%. Therefore, it is quite common to combine the mass–distance relations from adaptive optics (Equation (4)) and θ_E (Equation (2)) to measure the masses. This has been done on a number of planetary microlensing events (Janczak et al. 2010; Kubas et al. 2012; Batista et al. 2014, 2015; Bennett et al. 2015). In the favorable cases, it is possible to constrain the physical parameters of the system to within ≈5%. Recently, Koshimoto et al. (2017a) presented the discovery of a sub Saturn-mass planet and estimated the mass by combining parallax measurements (Equation (3)) and adaptive optics measurement, without a good measurement of θ_E. In this particular case, the accuracy of the parallax is the limiting factor determining the accuracy of the derived physical parameters. This is often the case for ground-based measurements, where only the parallax component parallel to the Earth acceleration is well measured, while the other is uncertain.

In order to overcome this limitation, a natural way forward is to obtain accurate parallaxes, by making simultaneous ground and space observations, as proposed first by Refsdal (1966) and further developed by Gould (1992). In contrast with observations from the ground alone, both components of the parallax vector could be well constrained. Three observing campaigns of simultaneous ground-based and *Spitzer* observations were completed in 2014–2016 (Yee et al. 2015a, 2015b; Calchi Novati et al. 2015).

2. The Planetary System OGLE-2014-BLG-0124

A very favorable case was OGLE-2014-BLG-0124, in which a system with a star plus planetary companion with mass ratio $q \sim 7 \times 10^{-4}$ and projected separation $d \sim 0.94$ was detected by the OGLE survey. It was observed simultaneously by a fleet of ground-based telescopes (MOA, LCOGT, Wise 1 m, MINDSTEP, and SAAO 1m), and by the *Spitzer* space telescope. It should be emphasized that this event was very favorable for parallax detection given its long timescale. During the ongoing microlensing event, models were circulated to characterize the nature of the event and optimize requests for complementary observations from follow-up telescopes.

Udalski et al. (2015) presented the analysis of OGLE and *Spitzer* data. OGLE captured the overall geometry of the microlensing light curve, a source transiting close to a resonant caustic. Although their model was ultimately based on OGLE and *Spitzer* data alone, it was completely consistent with the models created during the event, including data collected by the fleet of follow-up telescopes. Unfortunately, the original study failed to acknowledge this contribution from the community.

The OGLE data on its own allowed a π_E measurement to ±20%. The inclusion of *Spitzer* data improved this by a factor seven, making OGLE-2014-BLG-0124 the most precise microlensing parallax measurement to date. Unfortunately, the trajectory of the source star did not make any caustic crossings; Udalski et al. (2015) showed that t_* is uncertain, which transfers into a poorly known θ_E, and hence a large uncertainty on physical mass of the host star. It was also discussed by Yee (2015).

As a result, the system has two published solutions, which overlap within the errorbars. The first, for $u_0 > 0$, has an $M = 0.71 \pm 0.22\ M_\odot$ star located at 4.1 ± 0.6 kpc in the galactic disk, orbited by a planet of $M = 0.51 \pm 0.16\ M_{\mathrm{Jupiter}}$ at 3.1 ± 0.5 au; The second one ($u_0 < 0$), has an $M = 0.65 \pm 0.22\ M_\odot$ star located at 4.23 ± 0.59 kpc in the galactic disk, orbited by a planet of $M = 0.47 \pm 0.15\ M_{\mathrm{Jupiter}}$ at 2.97 ± 0.51 au. We remark that the microlensing parameters (mass ratio, projected separation) are very close and that the small difference in the physical parameters is coming mostly from the Bayesian modeling.

2.1. Source Star Properties

Udalski et al. (2015) fitted the source magnitude $I_S = 18.59 \pm 0.02$ with a bright blend contribution of $I_{\mathrm{Blend}} = 17.79 \pm 0.01$. They estimated the extinction to be $A_I = 1.02$, so $A_H = 0.236$ and $A_K = 0.17$, which leads to a dereddened source color of $(V-I)_{S0} = 0.70$. Using the relations in Bessell & Brett (1988), we derived $(I-H)_{S0} = 0.765$ and $(H-K)_{S0} = 0.055$. Knowing the extinction in the different bands, we predict the source magnitudes to be $H_S = 17.04 \pm 0.05$ and $K_S = 16.985 \pm 0.05$.

A direct measurement of the near-infrared magnitude of the source+lens therefore allows us to find the flux of the lens, and then to use Equation (4) to get a new mass–distance relation. We follow Bennett et al. (2015) and Beaulieu et al. (2016) to estimate the extinction toward the lens. We adopt as a scale height of the dust toward the galactic bulge $\tau_{\mathrm{dust}} = (0.120\mathrm{kpc})/\sin(|b|)$, where $b = -2.^\circ9167$ is the galactic latitude. Then we write the lens extinction A_{H_L}

$$A_{H_L} = (1 - e^{-D_L/\tau_{\mathrm{dust}}})/(1 - e^{-D_S/\tau_{\mathrm{dust}}})A_{H_S}. \quad (5)$$

2.2. VVV K-band Light Curve of OGLE-2014-BLG-0124

We extracted H and K cubes of images centered of the target collected by the 4 m VISTA telescope at Paranal during the VVV survey (Minniti et al. 2010). The data set is composed of 1 H and 312 K-band epoch. Using our standard procedure, we perform PSF photometry on all of the frames and calibrated them (Beaulieu et al. 2016; J.-B. Marquette et al. 2017, in preparation).

We use both VVV, OGLE, and *Spitzer* data to fit a binary-lens microlensing model using Markov Chain Monte Carlo, in order to double-check the initial study by Udalski et al. (2015) and to derive an estimate of the K_S band calibrated source flux

Table 1
Microlensing Model of OGLE-2014-BLG-124 Based on OGLE, VVV, and *Spitzer* Light Curves

Parameter	$u_0 > 0$	$u_0 < 0$
t_0 [HJD′]	6836.28 ± 0.04	6836.16 ± 0.03
u_0	0.176 ± 0.004	−0.174 ± 0.005
t_E [days]	150.8 ± 2.8	154.6 ± 4.2
$\rho[10^{-3}]$	0.88 ± 0.53	0.88 ± 0.52
π_{EN}	−0.005 ± 0.005	−0.015 ± 0.002
π_{EE}	0.145 ± 0.004	0.155 ± 0.006
α [rad]	4.510 ± 0.002	1.775 ± 0.002
ds/dt	−0.111 ± 0.015	−0.109 ± 0.017
$d\alpha/dt$	−0.7 ± 0.6	0.1 ± 0.6
s	0.944 ± 0.003	0.943 ± 0.004
q $[10^{-3}]$	0.69 ± 0.06	0.71 ± 0.05
I_s	18.60 ± 0.03	18.61 ± 0.04
K_s	16.93 ± 0.03	16.94 ± 0.04
χ^2	7017.1	7020.6

(see Figure 1). We perform these calculations for the two configurations described by Udalski et al. (2015), $u_0 > 0$ and $u_0 < 0$, corresponding to the two allowed trajectories of the source (Table 1) relative to the caustics. The microlensing parameters we find are in excellent agreement with those presented in Table 1 of Udalski et al. (2015), as they are all within 1σ. We derive K_S(fit) = 16.93 ± 0.03, with the blend magnitude K_b(fit) = 15.99 ± 0.01. This is in agreement with our estimates of $K_S = 16.985 \pm 0.05$ from the previous section.

As it is a direct measurement, we adopt in the following the fitted K-band source flux to be $K_S = 16.93 \pm 0.03$. The difference between the direct measurement and the extrapolation reflects the level of systematics errors in our procedure. We keep the H-band estimate with $H_S = 17.04 \pm 0.05$.

2.3. Keck II Adaptive Optics Observations of OGLE-2014-BLG-0124

On 2016 August 4, we observed OGLE-2014-BLG-0124 using NIRC2 mounted on the Keck II telescope on Mauna Kea. We used the wide camera, with a pixel scale of 0.04 arcsec. We took two frames with an exposure time of 3 × 10 s at each of the five dithered positions in H and K. We followed the data reduction and calibration procedures described by Beaulieu et al. (2016).

We correct for dark and flatfield using standard procedures and stack the images using SWarp from the Astr*O*matic suite of astronomy tools (Bertin 2010). We cross identify the VVV and the Keck II sources and estimate the calibration constant. We estimate the uncertainty on the zeropoint to be 0.008 mag in H and 0.01 in K. We apply this zeropoint to the Keck II catalogs.

We identify the source+lens star at the position marked on Figure 2. It has several blends at the ∼2 arcsec level. The total magnitude is $H_{VVV} = 15.75 \pm 0.07$ and $K_{VVV} = 15.66 \pm 0.10$ in the VVV images.

At the predicted position of the source, we measure $H_{Keck} = 15.95 \pm 0.04$ and $K_{Keck} = 15.79 \pm 0.03$. The PSF is slightly elongated due to the observing conditions; the ellipticity is identical to the PSF of nearby stars. As the source has $H_S = 17.04 \pm 0.05$ and $K_S = 16.93 \pm 0.03$, we estimate the blended light to be $H_{Blend} = 16.45 \pm 0.06$ and $K_{Blend} = 16.26 \pm 0.05$.

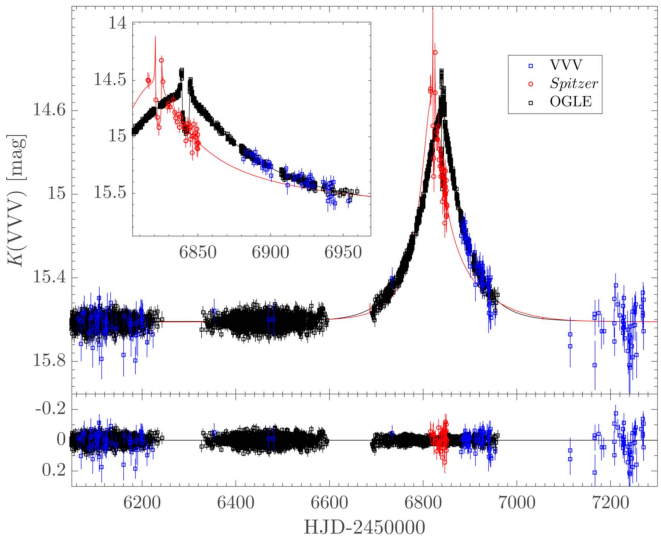

Figure 1. OGLE I band, *Spitzer*, and VVV K-band light curves and model of OGLE-2014-BLG-0124. We show the data, model, and residuals of the fit in the lower panel.

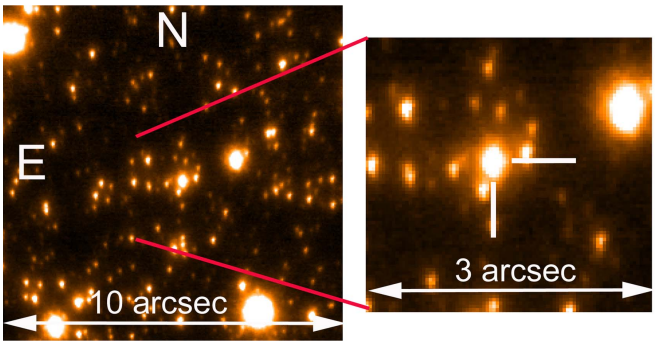

Figure 2. Keck II H-band observation of OGLE-2014-BLG-0124. At the position of the source, we detect significant additional flux within 150 mas, which is most likely the lens. The elongation seen on the image is consistent with the PSF shape of other nearby field stars.

3. Lens Star Properties

We detected blended light aligned with the source to an order better than the 160 milliarcsecond PSF full-width at half-maximum, so we must estimate if it is likely to be the lens star alone, or has contributions from:

1. the lens;
2. an ambient star (aligned with source and lens not associated with either;
3. a companion to the lens; and/or
4. a companion to the source.

We decided to compute the contribution to the blended light using two different methods and compare them.

3.1. Estimating Contaminants, Batista et al.'s Approach

We follow the Bayesian analysis described in V. Batista et al. 2018 in preparation. First, we calculate the probability for

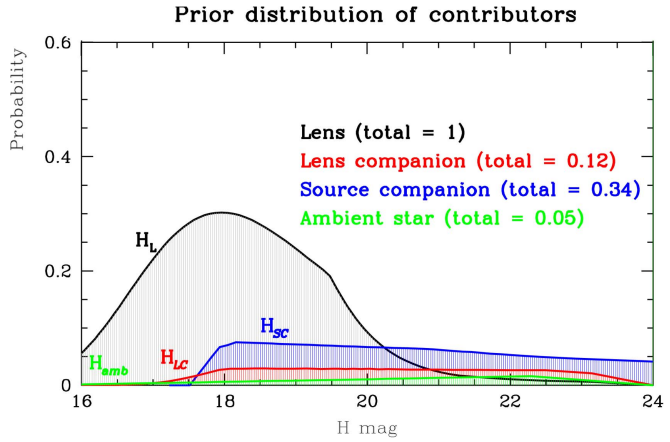

Figure 3. Prior distribution of contributors in H-band flux, lens, ambient star, companion to source, and companion to lens.

an unrelated star in the magnitude range $H = 15$–21 to be aligned by chance with the lens and the source. We assume that stars with a separation larger than $0.8 \times \mathrm{FWHM_{Keck}} = 130$ mas would be resolved. The probability of a field star contribution to the extra NIR flux is then equal to the surface number density of stars multiplied by the area ratio between a circle of 130 mas and the entire field.

While the upper limit to the separation is observationally given by $0.8 \times \mathrm{FWHM_{Keck}}$, the appropriate lower limits differ between a lens companion and a source companion. For a lens companion, we consider lower limits given the absence of signature from a source and a lens companion in the light curve, following the approach of Batista et al. (2014). We take a conservative lower limit to the separation by considering the upper limit on the microlensing shear that would be induced by an additional caustic,

$$\gamma = \frac{q}{s^2} < 10^{-3}.$$

For a source companion, the lower limit is given by the minimum separation for which the companion would not produce an additional perturbation in the light curve,

$$s \geqslant 1/4\, \theta_{\mathrm{E}} \sim 0.23 \text{ mas}.$$

The source and lens companions prior distributions of flux are calculated following the properties of binary star populations described by Duchêne & Kraus (2013, see V. Batista et al. 2017 in preparation for details). The distributions of the four potential contributors (lens, ambient star, source, or lens companion) are shown in Figure 3.

We combine the expected flux contributions from the four potentially luminous objects into 500,000 chains, weighted by their distributions and the Keck measurement. We extract a sample of the 1000 best fits and conclude that the most likely value of the lens contribution to the extra NIR flux is 85%. Figure 4 gives the posterior probability distribution of the sources of extra flux, with the inset showing the most probable contribution of each source to the detected object within a 160 mas separation.

3.2. Estimating Contaminants, Koshimoto et al.'s Approach

The same calculation has also been done following the approach of Koshimoto et al. (2017b); these authors also use the multiplicity estimates from Duchêne & Kraus (2013), but

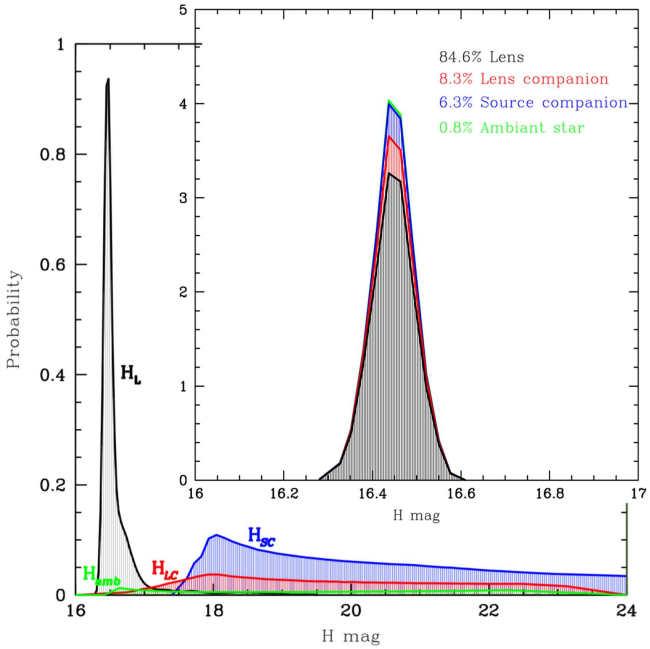

Figure 4. Posterior magnitude distribution of contributors to H-band flux: lens, ambient star, source companion, and lens companion. The insert shows the fraction of different flux sources accounting for the measured blended light. The dominant source is the lens, but companions to the source and the lens each have a significant expected contribution. Here, they account for 15% of the measured blended flux.

the treatment of the surface density distribution of field stars is slightly different. The two approaches also slightly differ in their a priori distributions: Koshimoto et al. (2017b) use a continuous law that is a function of the primary mass, whereas V. Batista et al. 2017 in preparation use a set of distinct laws associated to different mass bins.

Moreover, Koshimoto et al. (2017b) use a Galactic model in their calculation, while V. Batista et al. 2017 in preparation use the best-fit parameters from Udalski et al. (2015) for M, D_{L}, Π_{E}, and θ_{E}, and the OGLE calculator for D_{S}. Finally, the treatment of the Keck measurement in their Bayesian analysis slightly differs, as Koshimoto et al. (2017b) use it as a selection criteria of their flux combinations, while V. Batista et al. 2017 in preparation use it as an a priori distribution.

Nevertheless, prior and posterior distributions are very similar, and the fraction of the blended flux attributed to the lens is in agreement with the approach we adopted. The different contributions are estimated to be 79.3% for the lens, 2.4% for a chance-aligned star, 10% for a companion to the source, and 8% for a companion to the lens. This would lead to a lens less massive by $\sim 0.005\, M_{\odot}$ than using the approach adopted in the previous paragraph. We repeat the same calculation for the K-band data and obtain very similar results.

We conclude that the lens contributes to the great majority of the excess NIR flux detected in the Keck adaptive optics images, regardless of minor variations to the calculation of contamination probabilities.

4. Discussion and Conclusions

We estimated that 85% of the blended flux is due to the lens in H; therefore, $H_L = 16.63 \pm 0.06$. A similar result is obtained for K, so $K_L = 16.44 \pm 0.06$. We present in Figure 5 the constraints on mass and distance obtained for

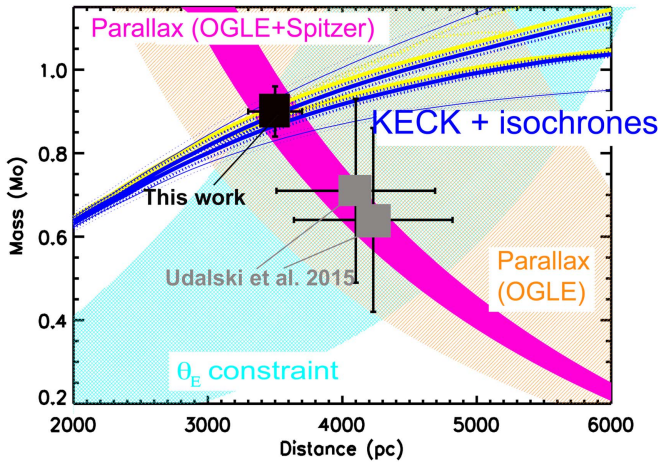

Figure 5. H-band isochrones in blue (Bertelli et al. 2008) for the $H_L = 16.63 \pm 0.06$ lens brightness for first planetary event with a *Spitzer* microlensing parallax measurement, OGLE-2014-BLG-0124. K-band isochrones for $H_K = 16.44 \pm 0.06$ are plotted in yellow. The parallax mass–distance relation from OGLE alone and OGLE + *Spitzer* are shown in orange and magenta, respectively. The mass–distance from Einstein ring radius θ_E estimate is shown in cyan. The gray squares mark the mass and distance estimates for the two solutions presented in the discovery paper. We plot our estimate as a black square with its error bar.

OGLE-2014-BLG-0124, via the three different routes summarized in Equations (2)–(4), namely: parallax, constraint on θ_E, and measuring the light from the lens. First, we use the mass–distance relation from θ_E and OGLE parallax; this gives a poor constraint on mass and distance of the system. However, the parallax constraint coming from OGLE combined with *Spitzer* is much stronger (drawn in pink). The gray squares indicate the two solutions for $u_0 > 0$ and $u_0 < 0$ presented by (Udalski et al. 2015), combining the accurate ground-space parallax with the mass–distance relation from θ_E (blue band). The latter constraint is quite weak due to the absence of caustic crossings in the source trajectory, with the consequent uncertain fitted value of t_*.

Our solution, plotted as a black square, relies on well determined parameters from adaptive optics measurements and *Spitzer* parallax and is in good agreement with the loose θ_E constraint. The lens star is an $M_L = 0.90 \pm 0.05\ M_\odot$ at a distance of $D_L = 3.5 \pm 0.2$ kpc. The microlensing fit gives two solutions, for $u_0 > 0$ and $u_0 < 0$. The parallax is nevertheless very close, as we get $\Pi_E = 0.148 \pm 0.0064$ and $\Pi_E = 0.146 \pm 0.006$, which give two mass–distance relations that are overlapping. The crossing of these constraints with the mass–distance relation coming from the detection of the lens gives the same solution for the lens mass. At this mass, the lens star would be a typical mid-late type main sequence star in the disk. Age constraints are weak, but most compatible with a typical age for disk stars, in the range ∼4–7 Gyr, assuming solar metallicity. Using the lens mass M_L, distance D_L, and the parallax Π_E we can recalculate that $\Theta_E(\mathrm{calc}) = 1.03 \pm 0.06$ mas, corresponding to 3.69 ± 0.21 au. We then use mass ratios and projected separation presented by Udalski et al. (2015) for the $u_0 > 0$ and $u_0 < 0$ cases. The two solutions for the physical parameters are very close (mutually consistent within errorbars), so we conclude that $M_p = 0.65 \pm 0.044\ M_{\mathrm{Jupiter}}$ at 3.48 ± 0.22 au.

This study shows the power of high angular resolution observations for constraining the host star properties in planetary microlensing events. It is also a cautionary tale showing that it is important to carefully estimate the potential contribution of source and lens companions that may potentially bias the inferred host properties if they are not accounted for. We note that for fainter lenses, these contributions will be more dramatic, like the case of MOA-2016-BLG-227 (Koshimoto et al. 2017b); a dedicated study will have to be performed in the framework of Euclid and WFIRST. Not accounting for these potential companions might lead to a bias toward higher inferred lens masses. In this case, because the lens star is bright, doing so would have resulted in a host mass $\sim 0.02\ M_\odot$ larger. This will become even more important in the case of fainter source and lens stars.

This work was supported by the University of Tasmania through the UTAS Foundation and the endowed Warren Chair in Astronomy. D.P.B. was supported by grant Nos. NASA-NNX12AF54G, JPL-RSA 1453175, and NSF AST-1211875. V.B. was supported by CNES. This work was partially supported by a NASA Keck PI Data Award, administered by the NASA Exoplanet Science Institute. Data presented herein were obtained at the W. M. Keck Observatory from telescope time allocated to the National Aeronautics and Space Administration through the agencies scientific partnership with the California Institute of Technology and the University of California. The Observatory was made possible by the generous financial support of the W. M. Keck Foundation. Work by Y.S. and C.H. was supported by an appointment to the NASA Postdoctoral Program at the Jet Propulsion Laboratory, California Institute of Technology, administered by Universities Space Research Association through a contract with NASA. This publication makes use of data products from the Two Micron All Sky Survey, which is a joint project of the University of Massachusetts and the Infrared Processing and Analysis Center/California Institute of Technology, funded by the National Aeronautics and Space Administration and the National Science Foundation. Work by N.K. is supported by JSPS KAKENHI grant No. JP15J01676. Work by D.D.P. and K.L. was supported by the University of Rijeka grant No. 13.12.1.3.02.

ORCID iDs

J.-P. Beaulieu https://orcid.org/0000-0003-0014-3354
V. Batista https://orcid.org/0000-0002-9782-0333
D. P. Bennett https://orcid.org/0000-0001-8043-8413
A. A. Cole https://orcid.org/0000-0003-0303-3855
A. Fukui https://orcid.org/0000-0002-4909-5763
N. Koshimoto https://orcid.org/0000-0003-2302-9562
D. Suzuki https://orcid.org/0000-0002-5843-9433
C. Henderson https://orcid.org/0000-0001-8877-9060
Y. Shvartzvald https://orcid.org/0000-0003-1525-5041

References

Batista, V., Beaulieu, J.-P., Bennett, D. P., et al. 2015, ApJ, 808, 170
Batista, V., Beaulieu, J.-P., Gould, A., et al. 2014, ApJ, 780, 54
Beaulieu, J.-P., Bennett, D. P., Batista, V., et al. 2016, ApJ, 824, 83
Bennett, D. P., Bhattacharya, A., Anderson, J., et al. 2015, ApJ, 808, 169
Bertelli, G., Girardi, L., Marigo, P., & Nasi, E. 2008, A&A, 484, 815
Bertin, E. 2010, SWarp: Resampling and Co-adding FITS Images Together, Astrophysics Source Code Library, ascl:1010.068
Bessell, M. S., & Brett, J. M. 1988, PASP, 100, 1134
Boyajian, T. S., von Braun, K., van Belle, G., et al. 2013, ApJ, 771, 40
Boyajian, T. S., von Braun, K., van Belle, G., et al. 2014, ApJ, 787, 92

Calchi Novati, S., Gould, A., Yee, J. C., et al. 2015, ApJ, 814, 92
Duchêne, G., & Kraus, A. 2013, ARA&A, 51, 269
Gould, A. 1992, ApJ, 392, 442
Gould, A., & Loeb, A. 1992, ApJ, 396, 104
Janczak, J., Fukui, A., Dong, S., et al. 2010, ApJ, 711, 731
Kervella, P., Bersier, D., Mourard, D., et al. 2004, A&A, 428, 587
Koshimoto, N., Shvartzvald, Y., Bennett, D. P., et al. 2017b, AJ, 154, 3
Koshimoto, N., Udalski, A., Beaulieu, J. P., et al. 2017a, AJ, 153, 1
Kubas, D., Beaulieu, J. P., Bennett, D. P., et al. 2012, A&A, 540, A78
Mao, S., & Paczynski, B. 1991, ApJL, 374, L37
Minniti, D., Lucas, P. W., Emerson, J. P., et al. 2010, NewA, 15, 433
Refsdal, S. 1966, MNRAS, 134, 315
Udalski, A., Yee, J. C., Gould, A., et al. 2015, ApJ, 799, 237
Yee, J. C. 2015, ApJL, 814, L11
Yee, J. C., Gould, A., Beichman, C., et al. 2015a, ApJ, 810, 155
Yee, J. C., Udalski, A., Calchi Novati, S., et al. 2015b, ApJ, 802, 76